

Critical phenomena in perfect fluids

David W. Neilsen and Matthew W. Choptuik

Center for Relativity, The University of Texas at Austin, Austin, TX 78712-1081

Abstract. We investigate the gravitational collapse of a spherically symmetric, perfect fluid with equation of state $P = (\Gamma - 1)\rho$. We restrict attention to the ultrarelativistic (“kinetic-energy-dominated”, “scale-free”) limit where black hole formation is anticipated to turn on at infinitesimal black hole mass (Type II behavior). Critical solutions (those which sit at the threshold of black hole formation in parametrized families of collapse) are found by solving the system of ODEs which result from a self-similar *ansatz*, and by solving the full Einstein/fluid PDEs in spherical symmetry. These latter PDE solutions (“simulations”) extend the pioneering work of Evans and Coleman ($\Gamma = 4/3$) and verify that the continuously self-similar solutions previously found by Maison and Hara *et al* for $1.05 \leq \Gamma \lesssim 1.89$ are (locally) unique critical solutions. In addition, we find strong evidence that globally regular critical solutions *do* exist for $1.89 \lesssim \Gamma \leq 2$, that the sonic point for $\Gamma_{\text{dn}} \simeq 1.8896244$ is a degenerate node, and that the sonic points for $\Gamma > \Gamma_{\text{dn}}$ are nodal points, rather than focal points as previously reported. We also find a critical solution for $\Gamma = 2$, and present evidence that it is continuously self-similar and Type II. Mass-scaling exponents for all of the critical solutions are calculated by evolving near-critical initial data, with results which confirm and extend previous calculations based on linear perturbation theory. Finally, we comment on critical solutions generated with an ideal-gas equation of state.

PACS numbers: 04.20.Dw, 04.25.Dm, 04.40.Nr, 04.70.Bw, 02.60.-x, 02.60.Cb

Submitted to: *Class. Quantum Grav.*

1. Introduction

The formation of black holes is an exciting topic in general relativity, and a class of solutions which exists precisely at the threshold of black hole formation has recently generated considerable interest. These solutions have surprising properties, reminiscent of some thermodynamic systems near phase transitions, and, by analogy, have been called critical solutions. Critical phenomena in gravitational collapse were first discovered empirically in simulations of the massless Klein-Gordon field minimally coupled to gravity (EMKG) [1]. Subsequent studies have shown that critical behavior is present in a variety of physical systems, and indicate that the phenomena are generic features of gravitational collapse in general relativity. In this paper we focus on the critical solutions for a spherically symmetric perfect fluid with equation of state $P = (\Gamma - 1)\rho$, where ρ is the total energy density and Γ is constant, and present new solutions for $\Gamma \gtrsim 1.89$. While we provide a brief introduction to critical solutions, the review by Gundlach is an excellent introduction to critical phenomena [2], and additional information can be found in [3].

1.1. Basic properties of critical solutions

Imagine an experiment to investigate the details of gravitational collapse and black hole formation by imploding shells of fluid with a fixed equation of state. The initial energy density in the shell might be

$$\rho = A_0 \exp \left[- (r - r_0)^2 / \Delta^2 \right], \quad (1)$$

where A_0 , r_0 , and Δ are parameters. In the course of the experiment we fix two of the three parameters, and allow only one of them, which we label p , to vary. For small p (assuming the fluid's initial kinetic energy is sufficiently large—i.e. in what one might call the ultrarelativistic limit), the fluid implodes through the origin and completely disperses. However, for p sufficiently large, in particular for p larger than some critical value p^* , a black hole forms during the implosion, trapping some of the matter/energy within a finite radius. In the exactly critical case, $p = p^*$, which represents the threshold of black hole formation, the evolution temporarily asymptotes to a special critical solution, Z^* , which has a number of interesting properties, including scale invariance (self-similarity) and universality. The critical solution is universal in the sense that if we now use different “interpolating families” to probe the threshold of black hole formation, we will generically find the same critical solution (provided we remain in the ultrarelativistic regime). Additionally, in the super-critical regime $p > p^*$, the black hole masses are well described by a scaling law

$$M_{\text{BH}}(p) \propto |p - p^*|^\gamma. \quad (2)$$

Here the mass-scaling exponent γ is *also* universal in the sense that it is independent of the particular choice of initial data family. (However, as first predicted by Maison [4], and Hara, Koike and Adachi [5, 6], and as discussed in detail below, γ *is* a function of the adiabatic index Γ .)

One of the most profound consequences of the self-similar nature of critical collapse is that black hole formation in the ultrarelativistic limit turns on at *infinitesimal* mass. In analogy with second-order phase transitions in statistical mechanics, we refer to this behavior as Type II. As we will discuss shortly, Type I behavior, wherein black hole formation turns on with *finite* mass in interpolating families, has also been seen in various models of collapse and it is undoubtedly present in at least some of the perfect fluid models considered here.

1.2. Critical solutions and one-mode instability

A crucial feature of the critical solutions sketched above is that they are, *by construction*, unstable. If this is not obvious, one should observe that the critical solution is *not* a long-time ($t \rightarrow \infty$) solution of the equations of motion. Indeed, as sketched above, the only long-time stable “states” one finds from evolutions of a generic ultrarelativistic family of initial data either have (i) all of the fluid dissipated to arbitrarily large radii, with (essentially) flat spacetime in the interior, or (ii) some fluid dissipated to arbitrarily large radii, with a black-hole in the interior. The critical solution, Z^* , on the other hand, exists just at the threshold of black hole formation, and, in near-critical evolutions, the dynamics asymptotes to Z^* *only* during the strong-field dynamical epoch. For any given initial data, this strong-field regime persists for a *finite* amount of time (as measured, for example, by an observer at infinity). Eventually (and in fact, on a dynamical time scale) any non-critical data will evolve into one of the two stable end states.

Although the unstable nature of critical solutions was clear from the earliest phenomenological studies, considerable insight has been gained from the observation by Koike, Hara and Adachi [7] that the “sharpness” of the critical behavior seen in Type II collapse suggests that the critical solutions have *exactly one* unstable mode in perturbation theory. This *ansatz* immediately explains the universality of the critical solution: as $p \rightarrow p^*$, one is effectively directly tuning out the single unstable mode from the initial data. Furthermore, using the self-similarity of the dynamics in the near-critical regime and a little dimensional analysis, it is an easy matter to relate the mass-scaling exponent to the Lyapunov exponent associated with the single mode. In fact, since the pioneering work by Koike *et al* , this picture of Type II critical solutions as one-mode unstable, self-similar “intermediate attractors” has been validated for essentially every spherically-symmetric model where Type II behavior has been observed in the solution of the full equations of motion.

Moreover, the perturbative analysis applies equally well to Type I critical solutions which, arguably, have been well known to relativists and astrophysicists for decades, although perhaps not in the context of interpolating families. In this case, the critical solution is an unstable *static* or *periodic* configuration which, depending on how it is perturbed, will either completely disperse, or collapse to a finite-mass black hole. Once again, one generically finds that such solutions have a *single* unstable eigenmode, whose Lyapunov exponent is now a measure of the increase in lifetime of the unstable configuration as one tunes $p \rightarrow p^*$. Type I behavior has been observed in the collapse of Yang-Mills [8] and massive scalar fields [9], and, as mentioned above, there is every reason to expect that it will occur in perfect fluid collapse. Indeed, it is well known that relativistic stellar models often exhibit a turn-over in total mass as a function of central density. Stars past this turn-over (generalized Chandrasekhar mass) are well known to be unstable, and, in fact, are almost certainly Type I solutions.

1.3. Critical solutions and self-similarity

Heuristically, systems exhibiting self-similarity appear identical over many different spatial and/or temporal scales, and generally arise in physical situations in which there are no natural length scales. Here it is important to note that a scale-free solution can be generated from a model which *does* have specific length scales, provided that the scaling solution represents a “self-consistent” limit. The current case of fluid collapse provides a perfect example. The rest mass of the fluid *does* set a length-scale, but the Type II critical solutions describe an ultrarelativistic limit wherein the rest-mass of the solution is irrelevant. To put this another way, we can have *solutions* of the equations of motion which have greater symmetry (scale symmetry in this case) than the equations of motion themselves.

Self-similarity can be either continuous (CSS) or discrete (DSS), and both types have been observed in critical gravitational collapse. The perfect fluid critical solutions have continuous self-similarity of the *first* kind, a particularly simple self-similarity wherein the solutions can be written solely as functions of dimensionless variables, such as $\zeta = r/t$, where r is the radial coordinate in spherical symmetry and t is the coordinate time. An example of a CSS function of the first kind is shown schematically on a spacetime diagram in figure 1.

At this point we should also note that the self-similar nature of Type II critical solutions provides a link between work on black-hole critical phenomena and the large body of literature dealing with self-similarity in the context of Einstein gravity

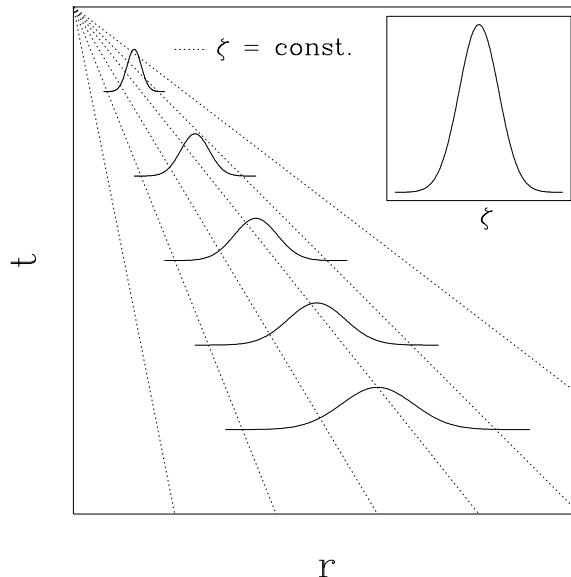


Figure 1. A schematic diagram showing a continuously self-similar (CSS) pulse at five different times as it moves toward the origin $r = 0$. The dotted lines are lines of constant $\zeta = r/t$, the similarity variable. These lines converge at the space-time origin $(r, t) = (0, 0)$ in the upper left-hand corner of the plot, and the inset shows the pulse as a function of ζ . As the pulse moves toward the origin, it appears the same on smaller and smaller length scales.

(see Carr and Coley [10] for a recent, extensive review). The self-similar *ansatz* has been widely employed, not only to produce more tractable problems, but also in investigations of possible mechanisms to generate counter-examples to the cosmic censorship conjecture. However, it is clear that not all self-similar solutions will be relevant to critical collapse, particularly if we restrict the definition of critical to “one-mode unstable”. Moreover, because most studies which are based on the self-similar *ansatz* have only considered the solutions themselves, and not perturbations thereof, it has proven non-trivial to identify which self-similar perfect-fluid solutions previously discussed in the literature are relevant to critical collapse [10, 11, 12].

1.4. Review of previous perfect-fluid studies

Shortly after the discovery of Type II behavior in scalar field collapse [1], Evans, having been frustrated in attempts to “analytically” understand the massless-scalar critical solutions, turned his attention to perfect-fluid collapse. Armed with the intuition that the self-similarity of critical collapse was a defining characteristic, and aware of the existence of continuously self-similar relativistic fluid flows, he and Coleman [13] considered collapse in the context of the specific equation of state, $P = \frac{1}{3}\rho$. Significantly, they were able to construct a single critical solution, both from the self-similar *ansatz* (i.e. by solving ODEs), and by tuning the initial data used in solution of the full partial differential equations of motion. Moreover, they noted that a perturbation analysis about the inherently unstable critical solution would provide an accurate description of the near-critical dynamics, including the calculation of the

mass-scaling exponent γ .

Such a perturbation analysis was quickly carried out (again for the case $P = \frac{1}{3}\rho$) by Koike *et al* [7], who, as mentioned above, made the crucial additional observation that the “sharp” transition in the mass scaling suggested that there was only *one* growing unstable mode associated with the critical solution, and that the Lyapunov exponent of the mode was simply the reciprocal of the mass-scaling exponent γ . Their analysis fully validated this conjecture—in particular, they found strong evidence for a single unstable mode with Lyapunov exponent 2.81055..., corresponding to $\gamma = 0.3558019...$, in excellent agreement with Coleman and Evans’ “measured” value, $\gamma \approx 0.36$.

At about the same time, Maison [4]—assuming that the critical solutions would be continuously self-similar for other values of Γ —adopted the CSS *ansatz* for the more general equation of state $P = (\Gamma - 1)\rho$. He was able to construct CSS solutions for $1.01 \leq \Gamma \leq 1.888$, and additionally presented strong evidence that all of the solutions were one-mode unstable. Furthermore, the Lyapunov exponents, and hence the mass-scaling exponents were found to be Γ -dependent, with, γ , for example, varying from $\gamma = 0.1143$ for $\Gamma = 1.01$ to $\gamma = 0.8157$ for $\Gamma = 1.888$. These calculations were particularly notable for providing early evidence that γ was not a “truly” universal exponent, in the sense of having the same value across *all* possible models of collapse.

One interesting outcome of Maison’s linearized analysis of the equations of motion about the sonic point, was that at $\Gamma \simeq 1.888$, two of the eigenvalues of the linearized problem degenerated, and the sonic point apparently changed from a node to a focus. This led Maison to conclude that regular self-similar solutions did not exist for $\Gamma \gtrsim 1.89$. A similar analysis by Hara, Koike and Adachi [5, 6] (expanding on their previous work) again suggested a change in solution behavior at $\Gamma \approx 1.89$. Those authors computed the CSS solutions, unstable eigenmodes, and eigenvalues for $1 < \Gamma \leq 1.889$, with results essentially identical to Maison’s. Evans and Perkins [14] also performed the linear stability analysis for $\Gamma \leq 1.888$, finding the same results reported by Maison. In addition, they performed the first critical solution searches using the full set of PDEs for $1.05 \leq \Gamma \leq 1.5$, confirming that the CSS solutions are the unique critical solutions for Γ in this range. Goliath *et al* [11] discussed, in the wider context of timelike self-similar fluid solutions, the mode structure of the $P = (\Gamma - 1)\rho$ CSS solutions, and reported that physical solutions do not exist for $\Gamma \gtrsim 1.89$. More recently, after this paper appeared in pre-print form, Carr *et al* have extended this work for $\Gamma \gtrsim 1.89$ [15, 16].

Furthermore, the conclusion of these linear perturbation analyses—that regular critical solutions for $\Gamma \gtrsim 1.89$ do not exist—has inspired various proposals regarding the nature of $\Gamma \gtrsim 1.89$ critical solutions [2, 10, 17]. (Recall that as long as we can set up interpolating data, there *will* be a critical solution, virtually by definition). One proposal is that a loss of analyticity at the sonic point for $\Gamma \gtrsim 1.89$ violates a condition required to find the ODE solutions. Other proposals have suggested that the solution might become Type I, discretely self-similar, or display a mixture of DSS and CSS behavior. Some of these conjectures were evidently based on the fact that, under certain conditions, a stiff ($P = \rho$) perfect fluid can be formally identified with the EMKG system [18, 19, 20]. For example, it has been conjectured [2, 10, 17] that at some point as $\Gamma \rightarrow 2$, the critical solution might begin to display the discrete self-similarity characteristic of the EMKG critical solution. Brady and Cai [17] have previously computed threshold solutions for $\Gamma \leq 1.98$ using the full fluid equations of motion, finding—in all cases examined—evidence that the critical solutions are

both CSS and Type II. Using a two-step Lax-Wendroff numerical scheme to integrate the fluid equations, they calculated mass-scaling exponents by evolving supercritical initial data. However their code has severe resolution limitations, being able to observe scaling only over two orders of magnitude in $|p - p^*|$.

Yet, lacking solutions for $\Gamma = 2$, and high resolution solutions near $\Gamma \simeq 1.89$, it was still expected that the perfect fluid critical solution changed its character as $\Gamma \rightarrow 2$. As we will discuss below, this does not seem to be the case, and in fact, $\Gamma \simeq 1.89$ seems problematic only in the context of the the precisely self-similar *ansatz*. Specifically, we have strong evidence that the CSS *ansatz* generates an increasingly ill-conditioned problem as $\Gamma \rightarrow 1.8896244\dots$, but that the PDEs remain perfectly well-behaved there.

1.5. Summary of results

Using a new perfect-fluid collapse code described in detail in [21], this paper examines the perfect fluid critical solutions for the full range of Γ , $1.05 \leq \Gamma \leq 2$, concentrating on those solutions for $\Gamma \gtrsim 1.89$. In addition to confirming the expected picture for $1.05 \leq \Gamma \leq 1.889$, we present further evidence that one-mode unstable CSS solutions exist in the regime $\Gamma \gtrsim 1.89$, up to and including, the limiting case $\Gamma = 2$. As part of this study, we are lead to re-investigate the CSS *ansatz*, and, in particular, the apparent change in solution behavior for $\Gamma \simeq 1.889$. In contrast to previous work, we solve the ODEs using arbitrary precision floating point arithmetic, which proves crucial to the analysis leading to our claim that the sonic points for $\Gamma \geq \Gamma_{\text{dn}} \simeq 1.8896244$ are *nodal* points, rather than *focal* points. We show that the CSS solutions for $\Gamma \gtrsim 1.89$ are qualitatively identical to those for $\Gamma \lesssim 1.89$, and verify that they can be computed from the full equations of motion (again using the code described in [21]). We also use simulations to compute mass scaling exponents in the regime $\Gamma \gtrsim 1.89$, where, interestingly, we find evidence to suggest that $\gamma \rightarrow 1$ as $\Gamma \rightarrow 2$.

Finally, researchers in this field have tacitly assumed that it suffices to consider $P = (\Gamma - 1)\rho$ in the context of critical collapse, since (1) the critical solution naturally “drives itself” to the ultrarelativistic (kinetic-energy-dominated) regime and (2) $P = (\Gamma - 1)\rho$ is the only equation of state compatible with self-similarity [22, 23]. We explicitly verify this assumption (albeit on a case-by-case basis) by performing computations—using an ideal-gas equation of state—which display the anticipated behavior.

2. Construction of the precisely critical solutions

Spherically symmetric perfect fluid critical solutions can be constructed by searching for globally regular, spherically symmetric, CSS solutions to Einstein’s equations [13]. As discussed in the Introduction, many studies of CSS perfect fluid spacetimes have appeared in the literature, and many properties of these solutions, such as their behavior near sonic points, are well known [4, 5, 10, 11, 22, 24, 25, 26, 27]. The self-similarity *ansatz* reduces the equations to first order, autonomous ODEs, and this section focuses on the solution of these ODEs for $\Gamma \gtrsim 1.89$. We use the equations derived by Hara *et al* [5], and refer the reader to that paper for additional information concerning the derivation of the equations, and basic methods for their solution.

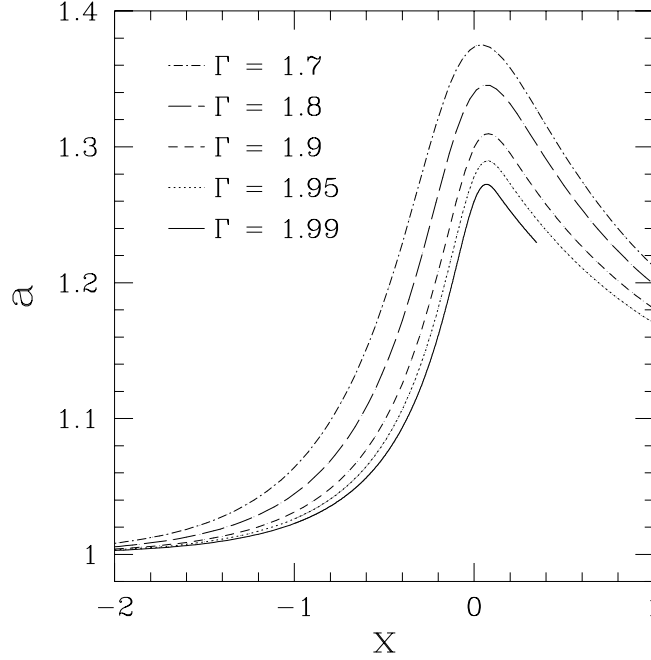


Figure 2. The geometric variable a of the critical solution for several values of Γ . The sonic point is at $x = 0$. The ODEs were integrated using the *Maple V* implementation of LSODE with 30 digits and an absolute error tolerance $\varepsilon = 10^{-18}$. We are increasingly unable to integrate these solutions outwards as $\Gamma \rightarrow 2$. This often occurs owing to a loss of numerical precision as $\omega \rightarrow 0$, and the Lorentz factor, $W = 1/\sqrt{1-v^2}$, becomes large (see figure 5).

2.1. The self-similarity ansatz

We write the spherically symmetric line element in polar-areal coordinates as

$$ds^2 = -\alpha(r, t)^2 dt^2 + a(r, t)^2 dr^2 + r^2 (d\theta^2 + \sin^2 \theta d\phi^2), \quad (3)$$

where the radial coordinate, r , directly measures the proper surface area. The Einstein equations give three relations for the metric quantities α and a (I:16)–(I:18) (equation numbers with a leading ‘I,’ refer to equations in [21]), and there are two fluid equations of motion (I:23). A continuously self-similar spacetime is generated by a homothetic Killing vector ξ [28],

$$\mathcal{L}_\xi g_{ab} = 2g_{ab}. \quad (4)$$

We impose the homothetic condition and introduce coordinates s and x adapted to this symmetry

$$s \equiv -\ln(-t), \quad x \equiv \ln\left(-\frac{r}{t}\right). \quad (5)$$

The time coordinate t is chosen such that the self-similar solution reaches the origin at $t = 0$, and the sonic point is at $x = 0$. We also define the dimensionless quantities

$$N \equiv \frac{\alpha}{ae^x}, \quad A \equiv a^2, \quad \omega \equiv 4\pi r^2 a^2 \rho. \quad (6)$$

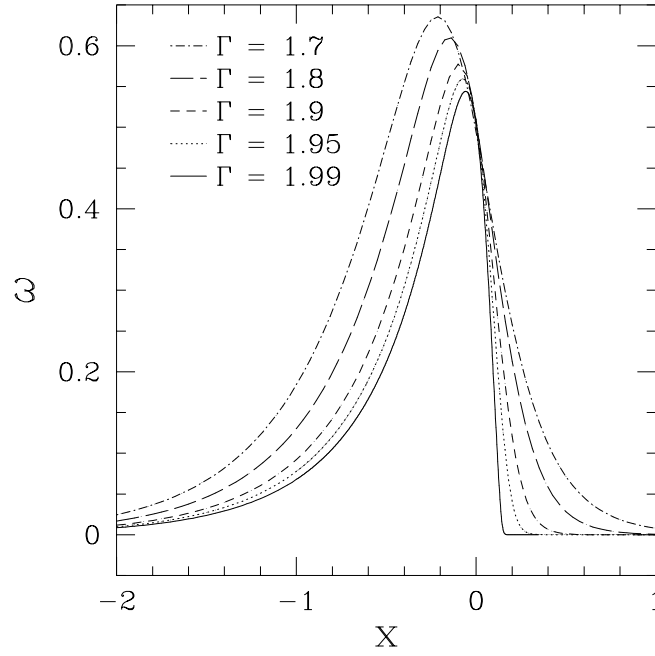


Figure 3. The fluid variable ω of the critical solution for several values of Γ . The sonic point is at $x = 0$.

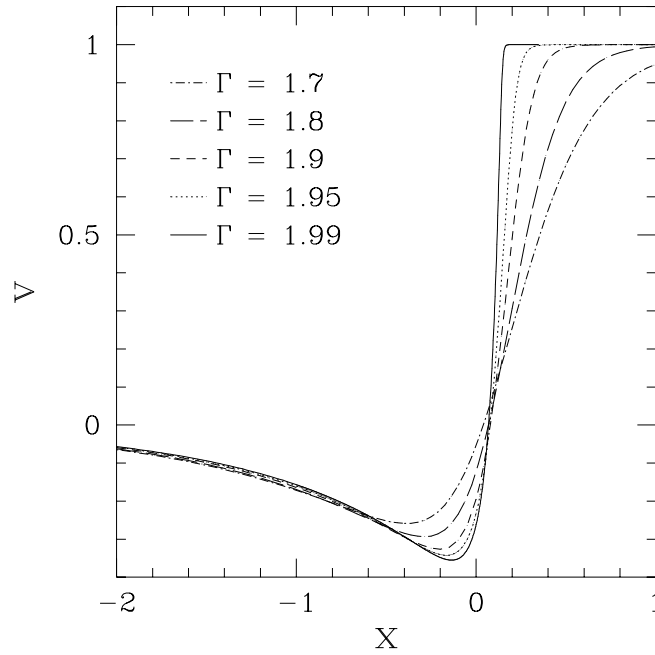


Figure 4. The fluid velocity v of the critical solution for several values of Γ . The sonic point is at $x = 0$.

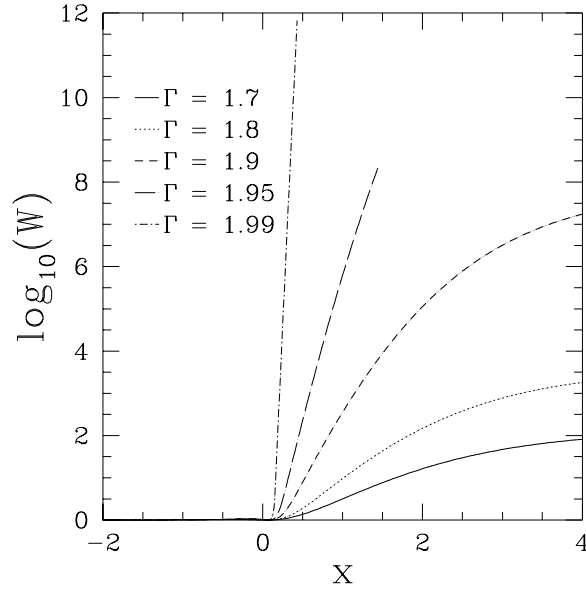


Figure 5. The logarithm of the Lorentz factor for the fluid velocity, $W = 1/\sqrt{1-v^2}$, of the critical solution for several values of Γ . Notice the exponential growth in the Lorentz factor for larger values of Γ . The sonic point is at $x = 0$.

The self-similarity *ansatz* requires that all derivatives with respect to s vanish, thus reducing the system to autonomous first order ODEs [5]. These equations are presented explicitly in Appendix A; here, we formally write them as

$$\mathcal{M}(y) y' = f(y), \quad (7)$$

where y is a “state vector” containing the four dependent variables $y^T = (A, N, v, \omega)$, \mathcal{M} is a 4×4 coefficient matrix, f is a “vector”, and a prime (') denotes differentiation with respect to x . By construction, all solutions of the ODEs (7) will be continuously self-similar; to find the unique critical solutions, we seek CSS solutions that are regular at both the origin and the sonic point [13].

2.2. The sonic point

The system of ODEs (7) can be solved provided that the inverse matrix \mathcal{M}^{-1} exists, that is, provided that the determinant [5]

$$\det \mathcal{M} \propto \frac{(1 + Nv)^2 - (\Gamma - 1)(N + v)^2}{1 - v^2}. \quad (8)$$

is non-zero. When $\det \mathcal{M} = 0$ —a condition occurring at a sonic Cauchy horizon or sonic point—the ODEs cannot be integrated without further assumptions. In particular, if $\det \mathcal{M} = 0$, the derivatives, y' , may either (i) not exist or (ii) be undefined. In the former case, the functions may be continuous but not differentiable, or a shock may form (discontinuous functions) at the sonic point; the latter case corresponds to the physically-relevant regular solutions in which we are interested. By definition, the sonic point is the position where the magnitude of the fluid velocity,

as measured by an observer at constant $x = \ln(-r/T)$, is equal to the fluid sound speed

$$c_s = \sqrt{\Gamma - 1}. \quad (9)$$

All CSS perfect fluid solutions that are regular at the origin have at least one sonic point [22]. If y is regular at the sonic point, then the rows of \mathcal{M} must be linearly dependent so that $\det \mathcal{M} = 0$. This condition allows one to parameterize the CSS solutions with a *single* parameter, v_{sp} , which is the fluid velocity at the sonic point. Furthermore, this regularity condition fixes y'_{sp} in terms of v_{sp} and v'_{sp} , yielding a quadratic condition on v'_{sp} which we schematically write as

$$c_2 v_{\text{sp}}'^2 + c_1 v'_{\text{sp}} + c_0 = 0. \quad (10)$$

Here, the coefficients, c_0 , c_1 and c_2 , are complicated functions of y_{sp} , and for simplicity of presentation will not be given explicitly. The key point is that this constraint—that the critical solutions are regular at the sonic point—limits the number of solutions to discrete values of v_{sp} , and virtually eliminates the possibility that globally regular solutions with more than one sonic point exist [22, 27]. Indeed, all of the $\Gamma \leq 2$ critical solutions we have found, either from a CSS *ansatz*, or by solving the full Einstein/fluid equations, have only one sonic point.

2.3. Solving the ODEs

The system of ODEs (7) is solved by choosing a candidate fluid velocity, v_{sp} , at the sonic point, and integrating numerically from the sonic point toward the origin. The inward integration is halted when either $A < 1$ or $\det \mathcal{M} = 0$, and these generic stopping criteria allow one to determine the parameter v_{sp} by a standard “shooting” procedure. (If $A < 1$ signals that v_{sp} is too small, then $\det \mathcal{M} = 0$ indicates that v_{sp} is too large, and vice versa). Once v_{sp} has been determined from the inward integration, the solution can be completed by integrating outwards from the sonic point. The entire solution process is complicated by the fact that the integration can not actually begin at the sonic point, since $\det \mathcal{M} = 0$ there. Therefore, we first expand the dependent variables y about the sonic point to first order

$$y_o \approx y_{\text{sp}} + y'_{\text{sp}} \Delta x, \quad (11)$$

where $\Delta x \equiv x_o - x_{\text{sp}}$, and actually begin the integration from x_o . Δx is chosen so that the $O((\Delta x)^2)$ error terms in the expansion, are smaller than the error tolerance allowed in the solution. We obtain y'_{sp} by solving (10) for v'_{sp} and integrate the ODEs for both roots.

The ODEs are integrated using **LSODE**, a robust numerical routine for integrating ODEs [29, 30], and *all* of the critical solutions can be found using double precision arithmetic, *except* those solutions for $\Gamma \approx 1.89$. These $\Gamma \approx 1.89$ solutions require greater precision, and can be found using the arbitrary precision implementation of **LSODE** in *Maple V*, which also proved invaluable for convergence testing the solutions. In the convergence tests we vary Δx , the **LSODE** absolute error tolerance ε (the relative error tolerance is set to zero), and the number of digits used in the calculation, while monitoring the residual of the algebraic constraint (A.6) as an indication of the error in the solution. For example, we calculated the critical solution for $\Gamma = 1.99$ using 40 digits and error tolerances $\varepsilon = 10^{-10}$, 10^{-15} , 10^{-20} and 10^{-25} , and then performed similar tests using 30 and 35 digits. In all cases the solutions converge, and the residual of (A.6) is $O(\varepsilon)$.

The critical solutions for several values of Γ are shown in figures 2–5. One notes that as $\Gamma \rightarrow 2$, it becomes increasingly difficult to integrate outwards from the sonic point, and this limitation is especially apparent in the Lorentz factors for the $\Gamma = 1.95$ and $\Gamma = 1.99$ critical solutions shown in figure 5. The ODE solver fails when the Jacobian matrix,

$$\mathcal{J} = \frac{\partial (\mathcal{M}^{-1}f)}{\partial y}, \quad (12)$$

becomes ill-conditioned, which often occurs when $\omega \approx \varepsilon$ and/or $v \approx 1 - \varepsilon$, where ε is the error tolerance supplied to **LSODE**. We can extend these solutions further outwards simply by increasing the number of digits used in the calculation. However the increase in maximum physical radius as a function of resolution is very modest—since the Lorentz factor W increases exponentially with increasing radius—and the process quickly becomes prohibitively expensive. Clearly, \mathcal{J} is always poorly conditioned near sonic points, but \mathcal{J} is particularly poorly conditioned near the sonic point for $\Gamma \approx 1.89$ —one can view this as a clear signal that numerical work will be difficult in the $\Gamma \approx 1.89$ regime.

2.4. Nature of the sonic point for $\Gamma \gtrsim 1.89$

Although nonlinear systems of ODEs are often impossible to solve in closed-form, qualitative features of their solutions can frequently be deduced by linearizing the equations about “critical” points. Perfect fluid CSS solutions have often been studied using this type of analysis [4, 5, 11, 22, 24, 25, 26, 27], and here we discuss some of these results in the context of our work. We emphasize, however, that we have *not* performed perturbation analyses in our current work.

The CSS perfect fluid equations (7) can be linearized about the sonic point, resulting in a system we can write in the form

$$y' = \mathcal{B}y, \quad (13)$$

where \mathcal{B} is a matrix which, generically, has two non-zero eigenvalues, which we label κ_1 and κ_2 (or simply κ when the distinction is irrelevant), with corresponding eigenvectors V_1 and V_2 . Near the sonic point, the solution of the linear equations (13) can be written [25]

$$y = y_{\text{sp}} + k_1 V_1 e^{\kappa_1 x} + k_2 V_2 e^{\kappa_2 x}, \quad (14)$$

where k_1 and k_2 are arbitrary constants. The eigenvalues κ provide important information about the solutions near the sonic point, and we classify the sonic point according to the relative values of κ , as given by the quantity ϑ [22]

$$\vartheta = \frac{\Gamma + \sqrt{\eta}}{\Gamma - \sqrt{\eta}}. \quad (15)$$

Here,

$$\eta \equiv 4(3\Gamma - 2)U^2 - (3\Gamma^2 - 12\Gamma + 8)(1 - 4U), \quad (16)$$

and

$$U \equiv \frac{A - 1}{2\omega}. \quad (17)$$

The sonic point classification in terms of ϑ is shown in table 1. Due to the facts that (i) ϑ is only a function of y_{sp} , and (ii) the eigenvalues κ are related to v'_{sp} [27],

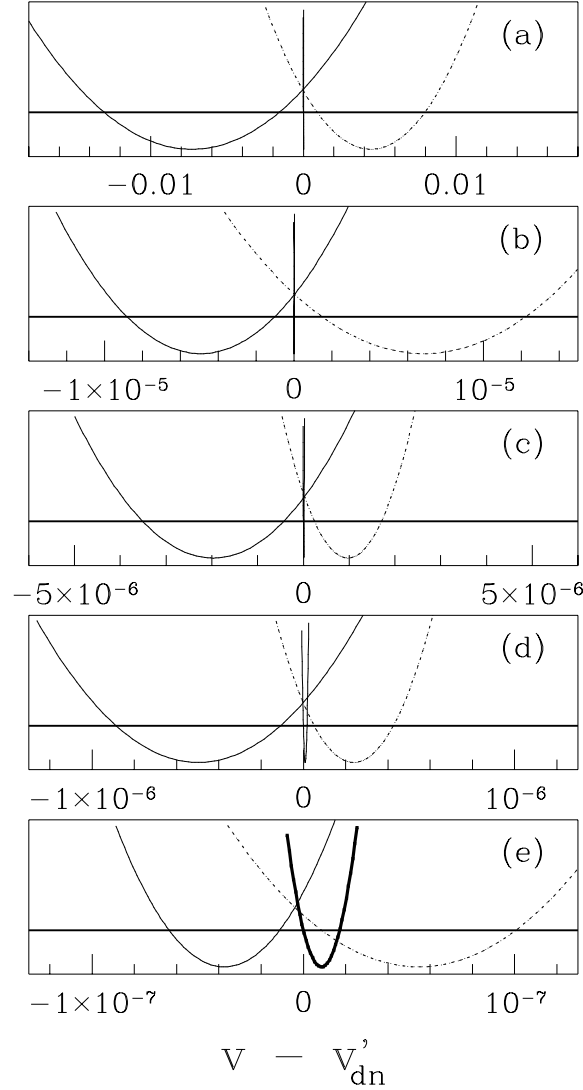


Figure 6. The sonic point of the $\Gamma_{\text{dn}} \simeq 1.8896244$ critical solution is a degenerate node, and this figure shows the approach to degeneracy by plotting the quadratic function in (10) as $\Gamma \rightarrow \Gamma_{\text{dn}}$. The roots of (10) are possible values for v' at the sonic point, and when $\Gamma = \Gamma_{\text{dn}}$ these roots are equal, v'_{dn} . Each frame shows a parabola for three values of Γ . The parabolas on the left are for Γ less than Γ_{dn} ($\Gamma_{<}$), and the parabolas on the right are for Γ greater than Γ_{dn} ($\Gamma_{>}$). The center parabola has the same Γ in all five frames, namely $\Gamma_C \simeq \Gamma_{\text{dn}}$ ($\Gamma_C = 1.88962441796875$), and one must be careful not to mistake it for a vertical axis in frames (a)–(c). For all Γ , the critical solution's v'_{sp} is the root closest to the center (v'_{dn}). We estimate $\Gamma_{\text{dn}} \simeq 1.8896244169921874$ ($v_{\text{sp}} = -0.18696\dots$, $v'_{\text{sp}} = 1.7385\dots$, and $\vartheta_{\text{sp}} = 1.0000000002$), and for clarity, we use v'_{dn} to translate the horizontal axis such that the parabolas cluster around zero, and normalize the parabolas. In frame (a), $\Gamma_{<} = 1.889$ and $\Gamma_{>} = 1.890$. In (b), $\Gamma_{<} = 1.889624$ and $\Gamma_{>} = 1.889625$. In (c), $\Gamma_{<} = 1.88962425$ and $\Gamma_{>} = 1.8896245$. In (d), $\Gamma_{<} = 1.889624375$ and $\Gamma_{>} = 1.8896244375$. In (e), $\Gamma_{<} = 1.889624410625$ and $\Gamma_{>} = 1.889624421875$. These calculations were done with *Maple V* using 30 digits and $\varepsilon = 10^{-18}$.

Table 1. Classifications of the sonic point using ϑ .

$\vartheta < 0$	saddle point
$\vartheta > 0$	nodal point
$\vartheta \in \mathbb{C}$	focal point
$\vartheta = 1$	degenerate nodal point

we can make a connection to the linearized theory without explicit calculation of the eigenvalues.

Maison [4] and Goliath *et al* [11] have previously concluded that the sonic points for $\Gamma \gtrsim 1.89$ are foci, with complex κ and v'_{sp} , and hence have suggested that physical self-similar solutions do not exist for $\Gamma \gtrsim 1.89$. (Hara *et al* did not address the existence of solutions for $\Gamma \gtrsim 1.89$, but presumably also encountered problems with their numerical analysis in that regime.) However, we find that $\vartheta > 0$ for *all* $\Gamma \gtrsim 1.89$ critical solutions, and thus conclude that the sonic-points for those solutions are nodes rather than foci. It seems plausible that this apparent contradiction stems from insufficient numerical precision in the earlier studies. To provide some specific evidence to back this claim, we have used *Maple* with 30 digits to find a critical solution for $\Gamma \simeq \Gamma_{\text{dn}}$. Then, taking v_{sp} from this solution, we have calculated ϑ using both 30 digits in *Maple* and **FORTRAN** double precision. The **FORTRAN** calculation gave a complex ϑ —which would support the erroneous (we claim) conclusion that the sonic point is a focus. The same calculation done with greater precision using *Maple* shows that the sonic point is actually a node. In addition, we find that for $\Gamma < \Gamma_{\text{dn}}$ (with Γ restricted to $\Gamma > 1.8$ for simplicity, and Γ_{dn} defined below), the critical solution's v'_{sp} is the maximum root of (10), while for $\Gamma > \Gamma_{\text{dn}}$, the critical solution's v'_{sp} is the minimum root. As $\Gamma \rightarrow \Gamma_{\text{dn}}$, the two roots v'_{sp} come closer together until they are equal for Γ_{dn} , as shown in figure 6. Here the sonic point is a degenerate node with $\Gamma_{\text{dn}} \simeq 1.8896244$ ($\eta_{\text{dn}} = \mathcal{O}(\varepsilon)$, and $\vartheta_{\text{dn}} = 1 + \mathcal{O}(\sqrt{\varepsilon})$).

3. Simulation of critical solutions

A crucial check that the CSS solutions of the ODEs are indeed the unique critical solutions involves a comparison with the solutions of the full Einstein/fluid equations. Although relativistic fluid equations are known to be difficult to solve (particularly relative to “fundamental-field” equations, such as the EMKG system), modern high-resolution shock-capturing schemes [31, 32, 33, 34] allow one to calculate flows with shocks of almost arbitrary strength. However, perhaps the greatest challenge in finding the perfect fluid critical solutions—especially as $\Gamma \rightarrow 2$ —is the accurate treatment of flows with very large Lorentz factors. In [21] we have outlined our computer program which solves the spherically-symmetric Einstein/fluid system, and using this code we have found the perfect fluid critical solutions for $1.05 \leq \Gamma \leq 2$. All of these solutions are continuously self-similar (CSS) and black hole formation for near-critical initial data begins with infinitesimal mass (Type II). In this section we compare the ODE and PDE solutions, discuss the mass-scaling exponents γ , and finally, briefly discuss critical solutions for the ideal-gas equation of state.

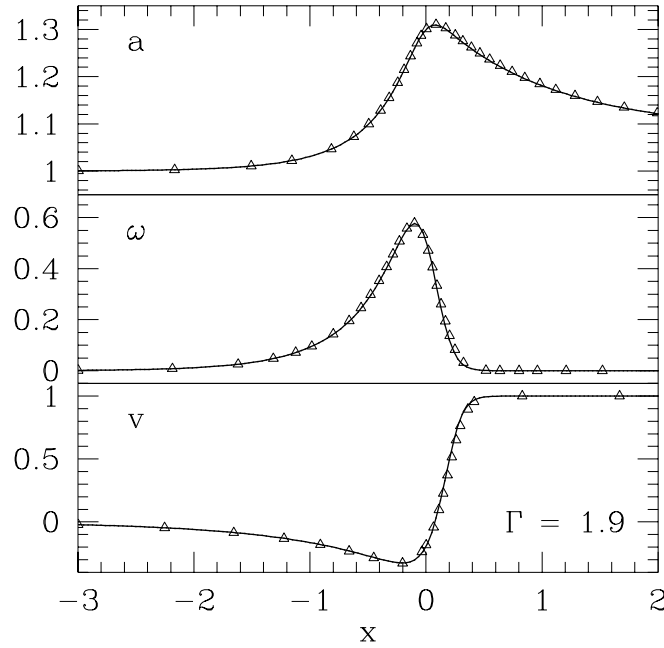


Figure 7. The $\Gamma = 1.9$ critical solution. The solid lines are the solution obtained by solving the ODEs, and the triangles indicate selected points from the solution of the PDEs.

3.1. Critical solutions

Figures 7–8 show the PDE critical solutions for $\Gamma = 1.9$ and $\Gamma = 1.99$ respectively, and include the ODE solutions for comparison. The $\Gamma = 1.9$ PDE and ODE solutions compare well, while figure 8 indicates that the $\Gamma = 1.99$ PDE solution underestimates a and ω . From our experience with other critical solution searches, we feel that this discrepancy is the result of insufficient (spatial) resolution. As $\Gamma \rightarrow 2$, the fluid becomes increasingly dynamic, requiring greater precision to resolve the solution’s relevant features, and it becomes increasingly expensive to calculate the critical solutions. The mass-scaling exponents γ shown in table 2 provide a quick guide to the requisite dynamical range for a critical evolution as $\Gamma \rightarrow 2$. As $(p - p^*)$ changes by n orders of magnitude, the relevant length scales in the solution, such as the radius of a black hole R_{BH} , change by γn orders of magnitude. The mass-scaling exponent for the stiff fluid, $\gamma \approx 1$, is almost three times larger than the scaling exponents for a radiation fluid ($\gamma \approx 0.36$) or massless scalar field ($\gamma_{\text{SF}} \approx 0.37$), and simulations of the stiff fluid critical solutions require correspondingly more resolution.

The critical solutions for $\Gamma < 2$ all appear very similar; indeed one can imagine that one could smoothly transform a solution for a given Γ into a solution for a different Γ . At first glance, the $\Gamma = 2$ solution seems to fit nicely into this “family” of critical solutions parameterized by Γ —it is CSS, Type II, and differs only slightly from the $\Gamma = 1.99$ critical solution. However, the ODE solution (obtained by solving ODEs with

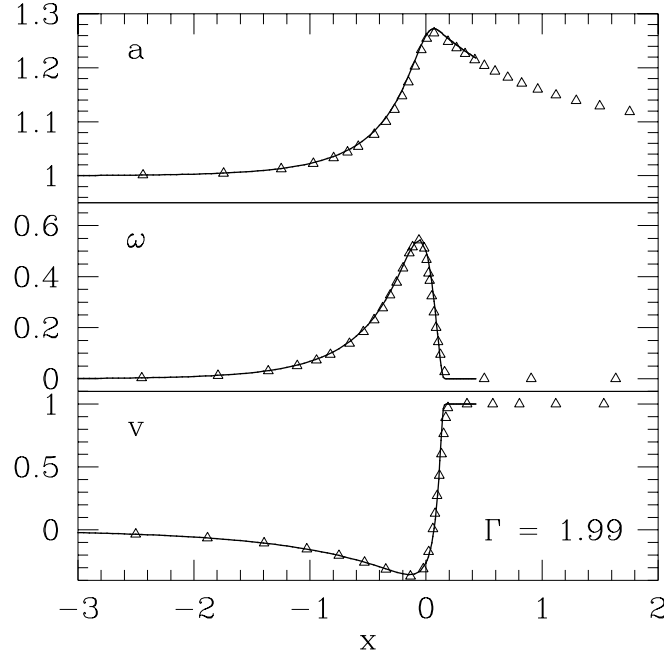


Figure 8. The $\Gamma = 1.99$ critical solution. The solid lines are the solution obtained by solving the ODEs, and the triangles are selected points from the PDE solution. The PDE solution underestimates the fluid density in the pulse leading, to a corresponding error in a . This problem stems from a lack of resolution in the computational grid.

the CSS *ansatz*) indicates that important differences may exist between the $\Gamma = 2$ and $\Gamma < 2$ critical solutions. As noted previously, we are unable to integrate the ODEs for Γ near 2 to arbitrarily large x . In these cases, we observe that the Lorentz factor, W , grows exponentially (see figure 5), with a corresponding exponential decrease in ω , until LSODE is unable to satisfy the required error tolerances. We emphasize that in these $\Gamma < 2$ solutions, the fluid velocity and density retains its expected “physical” properties: $\omega > 0$, and $|v| < 1$. The $\Gamma = 2$ solution (see figure 9), on the other hand, displays very different behavior. Instead of the exponential approach of $v \rightarrow 1$ and $\omega \rightarrow 0$, we find that ω and v pass through their expected physical bounds, giving $\omega < 0$ and $v > 1$. As is generally known, the stiff perfect fluid can be related to a scalar field, and, very recently, a CSS scalar field solution has been found by Brady and Gundlach that exactly matches the ODE $\Gamma = 2$ fluid solution [35].

The $\Gamma = 2$ PDE solution is also shown in figure 9, and in contrast to the ODE solution, this solution retains “physical” values for the fluid variables. However, this property of the PDE solution is achieved by *fiat*: we impose a “floor” on the fluid variables such that $\rho > 0$ and $|v| < 1$ [21]. While the floor is used generally for $\Gamma \gtrsim 1.8$ without noticeable ill effect for $\Gamma < 2$, it is clear that the floor affects the $\Gamma = 2$ solution (as compared to the ODE solution) even in the regime where $\omega > 0$

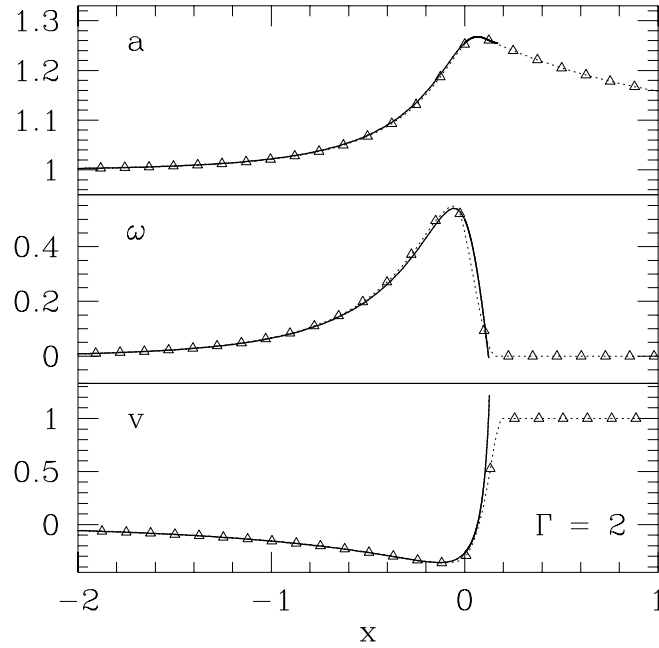


Figure 9. The $\Gamma = 2$ critical solution. The solid lines show the solution obtained from the ODEs, and the dotted lines with triangles show the solution obtained by solving the PDEs. Here some divergence between the PDE and ODE solutions can be seen. The PDE solution for ω lies *above* the ODE solution for $x < 0$, behavior opposite from that observed in the $\Gamma = 1.99$ solution. Beyond the sonic point, $x = 0$, the solutions become very different. Here the ODE solution becomes unphysical—in the traditional understanding of a perfect fluid—with $\omega < 0$ and $v > 1$. The PDE solution retains physical values for v and $\omega - v < 1$ and $\omega > 0$ —because these values are constrained to the physical regime in the evolution code [21].

and $|v| < 1$. The mathematical and physical significance of this observation is clearly an issue which requires more study—for example, can a vacuum region be matched to the $\Gamma = 2$ fluid in such a way that the fluid remains equivalent to a EMKG field [36]?

Finally, we note that the $\Gamma = 2$ critical solution is not related to other familiar EMKG solutions, such as the Roberts solution [37, 38], or the EMKG critical solution [1]. Both of these solutions have spacelike gradients of the scalar field. Extracting data from a near-critical $\Gamma = 2$ solution, we have set equivalent initial data for an EMKG evolution and then have evolved the data with the Einstein/scalar equations of motion. However, the evolution of the scalar field does *not* seem to match the $\Gamma = 2$ perfect-fluid critical solution for any appreciable length of time, and naïve variations of the initial data apparently produce the usual DSS scalar field critical solution at the black-hole threshold.

3.2. Mass-scaling exponents

Mass-scaling exponents γ are found by evolving near-critical initial data sets which lead to the formation of black holes. In our coordinate system, black hole formation is signaled by

$$\left. \frac{2m(r, t)}{r} \right|_{R_{\text{BH}}} \rightarrow 1, \quad (18)$$

where R_{BH} is the (areal) radius of the black hole. The black hole mass is then simply given by

$$M_{\text{BH}} = \frac{R_{\text{BH}}}{2}. \quad (19)$$

As mentioned earlier, all of the critical solutions discussed here are Type II, meaning that the associated black-hole transition begins with infinitesimal mass. As a typical example of our results, the mass-scaling of near-critical solutions for $\Gamma = 2$ is shown in figure 10.

The simple adaptive grid that we use [21] did not allow us to calculate M_{BH} with sufficient accuracy to justify searching for p^* to the limit of machine precision in a reasonable amount of time. We therefore estimated p^* by searching for the best linear fit to

$$\ln M_{\text{BH}} \propto \gamma \ln |p - p^*|. \quad (20)$$

The totality of mass-scaling exponents γ calculated from our simulation data are shown in table 2, along with the values predicted from Maison’s perturbative calculations [4]. (These exponents for $\Gamma \leq 1.98$ are similar to those found independently by Brady and Cai [17].) For a variety of reasons, estimation of the error (no doubt overwhelmingly “systematic”) in the mass-scaling exponents is not an easy task, and we therefore have provided estimates of γ which are conservative in their use of “significant” digits. One notes that as $\Gamma \rightarrow 2$, the mass-scaling exponent $\gamma \rightarrow 1$. This trend suggests that $\gamma = 1$ for $\Gamma = 2$. However our numerical results can only determine γ to very limited precision, and we are not currently aware of any argument for a precise equality.

3.3. Critical solutions for the ideal gas

The equation of state (EOS) $P = (\Gamma - 1)\rho$ can be interpreted as the ultrarelativistic limit of the ideal-gas EOS

$$P = (\Gamma - 1)\rho_o\epsilon, \quad (21)$$

where ρ_o is the rest energy density and ϵ is the specific internal energy density. Following Ori and Piran [22], Evans [23] (and others), we have argued [21] that self-similar perfect fluid solutions *require* the ultrarelativistic EOS. Let us now consider searching for critical solutions with the ideal-gas EOS. Heuristically, one can describe critical behavior in terms of competition between the fluid’s kinetic energy and gravitational potential energy. One might expect that in the critical solution, which stands just on the verge of black-hole formation, $P \gg \rho_o$, and that the critical solutions for the ideal-gas EOS would correspond to the ultrarelativistic EOS solutions. Using an evolution code, we have found critical solutions for the ideal-gas EOS, and these solutions *do* match the corresponding solutions with the ultrarelativistic EOS. As an example, the critical solution for a $\Gamma = 1.4$ ideal gas is compared with the precisely CSS ultrarelativistic $\Gamma = 1.4$ solution in figure 11. Additional evidence that near-critical ideal gas solutions are ultrarelativistic is shown in figure 12.

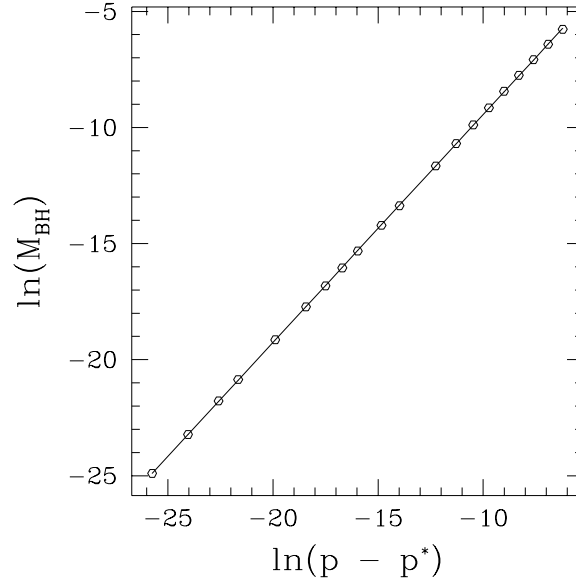


Figure 10. Illustration of black-hole mass scaling for the case $\Gamma = 2$. In this instance—as for all values of Γ considered here—the critical behavior is Type II, allowing one to create arbitrarily small black holes through sufficient fine-tuning of initial data.

Table 2. The mass-scaling exponent γ as a function of the adiabatic constant Γ . The second column shows the mass-scaling exponents estimated from $M_{\text{BH}}(p)$ by evolving near-critical ($p \rightarrow p^*$) initial data. For comparison, “calculated” exponents—computed from perturbative calculations—are also listed.

Γ	γ	
	Measured	Calculated ^a
1.05	0.15	0.1478
1.1	0.19	0.1875
1.2	0.26	0.2614
1.3	0.33	0.3322
4/3	0.36	0.3558
1.4	0.40	0.4035
1.5	0.48	0.4774
1.6	0.56	0.5556
1.7	0.64	0.6392
1.8	0.73	0.7294
1.888	0.82	0.8157
1.89	0.82	—
1.9	0.83	—
1.92	0.86	—
1.95	0.9	—
1.99	1	—
2	1	—

^a From Maison [4].

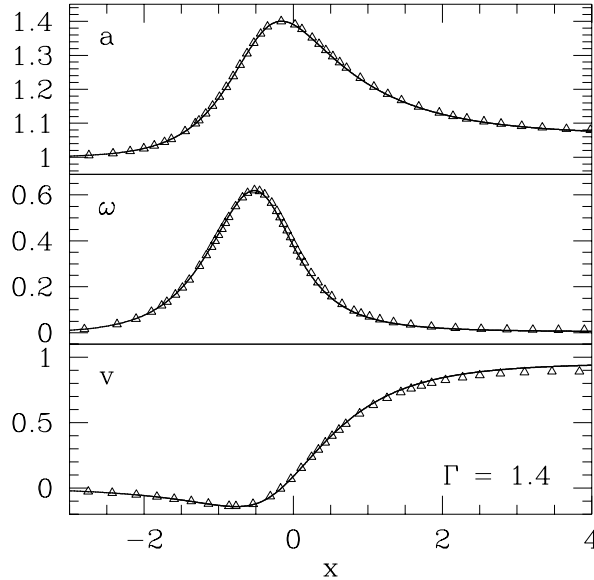


Figure 11. A comparison of the critical solutions for the ideal-gas and ultrarelativistic equations of state for $\Gamma = 1.4$. The solid lines are solutions obtained by solving the ODEs with the ultrarelativistic EOS, and the triangles are selected points from the PDE solution which uses the ideal-gas EOS. The ideal gas is in the ultrarelativistic limit near the infalling matter (see figure 12), and the two solutions correspond in this region. At large r the ultrarelativistic approximation breaks down, and the solutions differ. The ideal-gas EOS solution was computed using a code similar to the one described in [21].

4. Conclusion

Following seminal work by Evans and Coleman [13], Maison [4], and Hara, Koike and Adachi [5] have previously reported the existence of CSS solutions with a single unstable (relevant) mode for $\Gamma \lesssim 1.89$. In this paper we have shown that such solutions also exist for $\Gamma \gtrsim 1.89$, and have found evidence that the sonic point is a degenerate *node* for the $\Gamma_{\text{dn}} \simeq 1.8896244$ critical solution. Our results come from (i) a demonstration of the existence of globally regular CSS solutions for $\Gamma \leq 2$ (starting from a CSS *ansatz*), and (ii) the evolution of finely-tuned initial data in full simulations of the Einstein/fluid equations. The simulations verify that the CSS solutions sit at the threshold of black hole formation, and also allow us to compute mass scaling exponents which are in good agreement with predictions from perturbation theory. The $\Gamma = 2$ critical solution is also CSS and Type II, with a mass-scaling exponent very close to (if not identical to) unity. We have also investigated critical collapse using the ideal-gas equation of state, and, as expected, have found that the fluid *is* well-described in the near-critical regime by an ultrarelativistic approximation, and thus has critical solutions identical to those generated using $P = (\Gamma - 1)\rho$.

While we have addressed some of the questions regarding the $\Gamma \gtrsim 1.89$ critical solutions that have appeared in the literature, other avenues for further research

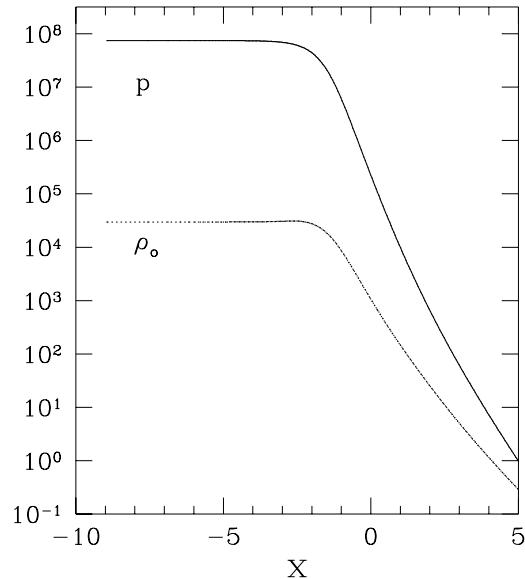


Figure 12. P and ρ_o are shown at the moment of maximum compression in this log-log plot of a marginally subcritical evolution of a $\Gamma = 1.4$ ideal gas. Note that near the origin, the ideal gas is clearly in the ultrarelativistic limit where $P \gg \rho_o$. At large r (X), the ultrarelativistic limit no longer holds, and the solution does not match one computed using the ultrarelativistic EOS.

remain. Perhaps foremost is the need for a greater understanding of the $\Gamma = 2$ critical solution, both in a more precise estimate of its mass-scaling exponent, and its precise relation to the EMKG field. In addition, Gundlach [39] and Martin-Garcia and Gundlach [40] have recently investigated the critical behavior of an axisymmetric radiation fluid with angular momentum. Full simulations of such scenarios will undoubtedly yield further interesting results.

Finally, we wish to point out an obvious use of critical solutions for testing and benchmarking new codes which solve the equations of motion (PDEs) for general relativistic fluids. In particular, we are unaware of widely-used test-bed solutions which combine both dynamic fluid flows *and* strong gravitational fields. Common tests for such codes currently include Riemann shock tube configurations, static Tolman-Oppenheimer-Volkoff solutions and Oppenheimer-Snyder dust collapse. The former tests lack gravitational effects, and the latter tests lack either dynamic fluid flows or pressure effects. While we do not advocate abandoning traditional tests, we wish to emphasize that critical solutions are novel in that they combine several computationally challenging characteristics: extremely relativistic and dynamic fluid flows, strong gravitational field dynamics, and relevant features over many space/time scales. In particular, as adaptive mesh refinement (AMR) becomes available for multi-dimensional simulations, these features should make critical solutions ideal candidates for code calibration.

Acknowledgments

This work was supported in part by the National Science Foundation under Grants PHY93-18152 (ARPA supplemented), PHY94-07194, PHY97-22068, by a Texas Advanced Research Project grant, and by an NPACI award of computer time. We thank P. Brady, D. Garfinkle, M. Goliath, C. Gundlach, and D. Maison for helpful discussions and suggestions, and are particularly indebted to M.R. Dubal for his substantial contributions to an earlier (and unpublished) attack on the problem of perfect-fluid critical collapse. MWC gratefully acknowledges the hospitality of the Institute for Theoretical Physics, UC Santa Barbara, where part of this research was carried out.

Appendix A. ODEs for a self-similar spacetime

The Einstein equations for a spherically symmetric, CSS perfect fluid are presented in this appendix for reference. These equations are derived in [5].

$$\frac{A'}{A} = 1 - A + \frac{2\omega(1 + (\Gamma - 1)v^2)}{1 - v^2} \quad (\text{A.1})$$

$$\frac{N'}{N} = -2 + A - (2 - \Gamma)\omega \quad (\text{A.2})$$

$$\frac{A'}{A} = -\frac{2\Gamma N v \omega}{1 - v^2} \quad (\text{A.3})$$

$$\begin{aligned} (1 + Nv) \frac{\omega'}{\omega} + \frac{\Gamma(N + v)v'}{1 - v^2} \\ = \frac{3}{2}(2 - \Gamma)Nv - \frac{2 + \Gamma}{2}ANv + (2 - \Gamma)Nv\omega \end{aligned} \quad (\text{A.4})$$

$$\begin{aligned} (\Gamma - 1)(N + v) \frac{\omega'}{\omega} + \frac{\Gamma(1 + Nv)v'}{1 - v^2} \\ = (2 - \Gamma)(\Gamma - 1)N\omega + \frac{7\Gamma - 6}{2}N + \frac{2 - 3\Gamma}{2}AN \end{aligned} \quad (\text{A.5})$$

The equations (A.2)–(A.5) are integrated to find the critical solutions, and comprise the system $\mathcal{M}y' = f$ in (7). Equations (A.1) and (A.3) can be combined to give an algebraic constraint

$$(1 - A)(1 - v^2) + 2\omega(1 + (\Gamma - 1)v^2) + 2\Gamma N v \omega = 0. \quad (\text{A.6})$$

This equation is *not* used to integrate the ODEs, but is monitored during the integration as an indication of the error in the solution.

References

- [1] Choptuik M W 1993 *Phys. Rev. Lett.* **70** 9
- [2] Gundlach C 1998 *Adv. Theor. Math. Phys.* **2** 1; [gr-qc/9712084](#)
- [3] Choptuik M W 1998 [gr-qc/9803075](#)
- [4] Maison D 1996 *Phys. Lett. B* **366** 82
- [5] Hara T, Koike T, and Adachi S 1996 [gr-qc/9607010](#)
- [6] Koike T, Hara T, and Adachi S 1999 *Phys. Rev. D* **59**
- [7] Koike T, Hara T and Adachi S 1995 *Phys. Rev. Lett.* **74** 5170

- [8] Choptuik M W, Chmaj T and Bizon P 1996 *Phys. Rev. Lett.* **77** 424
- [9] Brady P 1997 [gr-qc/9709014](#)
- [10] Carr B J and Coley A A 1998 [gr-qc/9806048](#)
- [11] Goliath M, Nilsson U S and Uggla C 1998 *Class. Quantum Grav.* **15** 2841
- [12] Carr B J and Coley A A 1999 [gr-qc/9901050](#)
- [13] Evans C R and Coleman J S 1994 *Phys. Rev. Lett.* **72** 1782
- [14] Perkins T J W 1996 thesis (unpublished)
- [15] Carr B J, Coley A A, Goliath M, Nilsson U S and Uggla C 1999 [gr-qc/990131](#)
- [16] Carr B J, Coley A A, Goliath M, Nilsson U S and Uggla C 1999 [gr-qc/990270](#)
- [17] Brady P R and Cai M J 1998 [gr-qc/9812071](#)
- [18] Taub A H 1959 *Arch. Rat. Mech. Anal.* **3** 312
- [19] Madsen M K 1985 *Astrophys. Space Sci.* **113** 205
- [20] Madsen M K 1988 *Class. Quantum Grav.* **5** 627
- [21] Neilsen D W and Choptuik M W 1998 submitted to *Class. Quantum Grav.*
- [22] Ori A and Piran T 1990 *Phys. Rev. D* **42** 1068
- [23] Evans C R 1993 in *Lecture Notes of the Numerical Relativity Conference, Penn State University, 1993* (unpublished)
- [24] Bogoyavlenskii O I 1977 *Sov. Phys. JETP* **46** 633
- [25] Bicknell G V and Henriksen R N 1978 *ApJ* **219** 1043
- [26] Bicknell G V and Henriksen R N 1978 *ApJ* **225** 237
- [27] Foglizzo T and Henriksen R N 1993 *Phys. Rev. D* **48** 4645
- [28] Cahill M E and Taub A H 1971 *Comm. Math. Phys.* **21** 1
- [29] Hindmarsh A C 1983, in *Scientific Computing* Stepleman R S *et al* (eds.) (North-Holland, Amsterdam) 55
- [30] Petzold L R 1983 *J. Sci. Stat. Comput.* **4** 136
- [31] LeVeque R J 1992 *Numerical Methods for Conservation Laws* (Birkhäuser-Verlag, Basel)
- [32] LeVeque R J 1998 , in *Computational Methods for Astrophysical Fluid Flow*, 27th Saas-Fee Advanced Course Lecture Notes (Springer-Verlag, Berlin, to be published); also available at <http://sirrah.astro.unibas.ch/saas-fee/>.
- [33] Ibáñez J M^a, Martí J M^a, Miralles J A and Romero J V 1992 *Approaches to Numerical Relativity*, (Cambridge University Press, Cambridge) p 223.
- [34] Romero J V, Ibáñez J M^a, Martí J M^a and Miralles J A 1996 *ApJ* **462** 839
- [35] Brady P, Gundlach C, Neilsen D, and Choptuik M 1999 in preparation
- [36] Gundlach C 1999 personal communication
- [37] Roberts M D 1985 *Gen. Rel. Grav.* **17** 913
- [38] Roberts M D 1998 [gr-qc/9811093](#)
- [39] Gundlach C 1998 *Phys. Rev. D* **57** 7080
- [40] Martin-Garcia J M and Gundlach C 1998 [gr-qc/9809059](#)